Measured temperature effects during the construction of a prestressed precast concrete bridge beam

Frank Küsel[1], *Elsabe* Kearsley[1,*], *Liam J.* Butler[2], *Sarah A.* Skorpen[1], *M.Z.E.B.* Elshafie[2]

[1]Department of Civil Engineering, University of Pretoria, Pretoria, South Africa
[2]Department of Engineering, University of Cambridge, UK

ABSTRACT. Prestress losses in precast concrete beams include the short-term effects of elastic shortening and the long-term effects of concrete shrinkage, concrete creep and steel relaxation. Temperature effects are, however, excluded. The aim of this research was to monitor the behaviour of a prestressed precast concrete bridge beam, focussing on temperature effects and destressing. Successful monitoring assists in comparing the real performance of a structure to the expected design performance, and in managing the durability of the monitored structure. The effect of temperature variation on strains in prestressed beams was investigated by instrumenting a precast beam. Temperature and strains were monitored from the day of casting up to and including the cutting of the pretensioning strands. Daily temperature variations causing vertical non-linear temperature profiles resulted in internal strains of up to 28 % of the strains caused by destressing. It was therefore concluded that thermal effects before destressing resulting from elevated curing temperatures and daily temperature changes should be considered in the calculation of prestress losses. The monitoring techniques used were successful in determining the stresses and strains within the beam, which can be used to compare real prestress losses with the losses assumed in design.

1 Background and Introduction

Temperature changes in prestressed precast concrete beams induce thermal stresses by way of either an overall temperature change of the beam, resulting in longitudinal changes in length, or non-linear temperature gradients in the cross-section of the beam, resulting in internal strain differentials. Although temperature effects are ignored in prestress losses, they can affect the stresses, strains and camber of a bridge during fabrication and service [1]. Underestimating prestress losses can result in excessive deflection or cracking, leading to decreased durability.

1.1 Thermal effects in bridges

Previous studies on thermal effects in structures mostly included concrete and steel composite bridges [2-5], while fewer researchers looked at prestressed bridges and their thermal behaviour. Thermal gradients caused by weather conditions were investigated by Gilland and Dilger [6] and Pisani [7], whilst Li et al [8] investigated different theoretical thermal gradients. Lee et al. [9] developed methods to calculate maximum lateral and vertical deflections from daily climatic information. Lee [10] determined the behaviour of a pretensioned beam before placement using 3D nonlinear finite element analysis.

In addition to vertical temperature gradients, Emmerson [11] described the longitudinal bridge movements as a result of an effective temperature of the bridge. The effective temperature is based on the mean temperature of different isotherms and their respective cross-sectional areas. Dwairi et al. [12] showed that thermal effects were the main cause of in service girder end displacements and not traffic loading. Furthermore, Roeder et al. [5] indicated that the longitudinal bridge movements caused by mean bridge temperatures can cause large transverse moments in bridges that are built obliquely between abutments. An increase in the angle increases the transverse moments, particularly in short spans.

Imbsen et al. [13] recommends standard temperature gradients to be used in designing for thermal effects. These thermal effects depend significantly on the cross-section geometry and great care must be taken in assuming a specific temperature gradient. Emmerson [14] discussed design requirement guidelines for temperature differences in bridges. Different temperature gradients are given in the vertical direction through the depth of the deck for various concrete decks. The mechanisms for heat transfer described by Roeder et al. [5] include sun radiation, surface radiation, convection and conduction. Roeder et al. [5] showed that these thermal effects can result in additional extreme fibre

* Corresponding author: elsabe.kearsley@up.ac.za

stresses which affects the requirements for longitudinal reinforcing.

1.2 Thermal effects in precast prestressed beams

Butler et al. [15] monitored temperature and strains during and after casting, and in service using distributed and discrete fibre optic networks. Butler et al. [15] and Dwairi et al. [12] both observed compression in the concrete following the completion of concrete hydration followed by a gradual decrease in compressive strains. The top and bottom strains of the beam were not the same after hydration, indicating locked in strains which are important when evaluating prestress losses that result from elastic shortening during detensioning [15].

Barr et al. [16] calculated prestress losses of up to 26 % and a 40 % reduction in expected camber as a result of elevated curing temperatures. Strands stressed at ambient temperatures are heated by the higher temperatures of concrete hydration, causing the stress in the strand to decrease as they are anchored at the ends. Riding et al. [17] showed that early-age thermal stresses were also introduced because of different concrete pouring times, with up to 46% reduction in stresses when casting at different daily temperature extremes. The calculated stresses were based on the recorded strains and the Young's Modulus of the concrete.

Temperature changes of the steel strands should be included in the calculation of prestress losses [18]. The temperature at the time of stress transfer from the strands to the concrete may also affect the amount of prestress losses [19]. Theoretical models for the prestress losses caused by only a change in temperature of the tendons indicated a prestressing force change between 3 and 5 % percent [20]. The variability in predicted prestress losses is a consequence of the many influencing factors, including the coefficient of thermal expansion, the modulus of elasticity, curing temperatures, aggregate type and cross-section geometry. The modulus of elasticity of concrete varies greatly and depends on the aggregate, moisture content and temperature at the time of mixing and curing. In addition to the modulus of elasticity, the differences in the coefficient of thermal expansion between the concrete and the steel, the temperature gradient and the time at which the concrete bonds to the strands affects the magnitude of the prestress losses and the camber [16].

The age of the concrete (which is dependent on time and temperature) for cutting the prestressing strands and installing the beam is also important when calculating prestressing losses [15]. Since temperature induced strains depend on the material properties, thermal stresses were shown to be sensitive to the coefficient of thermal expansion of the concrete [1,17].

Based on the previous studies, it is evident that temperature effects are introduced into the structure throughout all stages of construction and service. However, little research has been conducted on the temperature induced strains and their influence before the pretensioning strands are cut. This paper presents the monitoring data captured during the fabrication of a precast prestressed beam and analyses the effect of temperature on the instantaneous prestress losses.

2 Experimental Setup

A precast prestressed concrete bridge beam as indicated in Figure 1 was instrumented to monitor the stresses and strains experienced by the beam throughout the construction stages and throughout its service life. The geometry of the instrumented precast beam is shown in Figure 2. The beam is 32.6 m long and it will be used in a bridge which crosses a road at an angle. The diaphragms and edge faces of the beam are therefore not perpendicular to the length of the beam. There are 54 prestressing strands located in the beam as shown in Figure 2.

Fig. 1. Precast prestressed concrete beam.

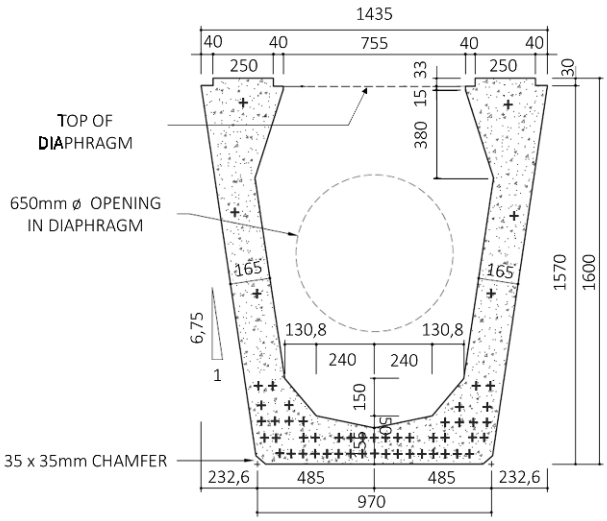

Fig. 2. Beam cross-section.

2.1. Material Properties

Material properties were determined using concrete samples taken during the concrete pour and prestressing strand properties were obtained from the manufacturer. Table 1 shows the concrete and steel properties.

Table 2. Material Properties

	Concrete	Steel	Steel Strands
Characteristic Strength f (MPa)	58.1	450	1880
Young's Modulus E (GPa)	43.5	200	198
Coefficient of Thermal Expansion α (με/°C)	8.8	12	12

2.1. Instrumentation Layout

The daily temperature and strain cycles were recorded before and during the cutting of the prestressing strands, from the time of casting. Vibrating Wire Strain Gauges (VWSG), thermistors and discrete fibre optics sensors (i.e. fibre Bragg gratings or FBGs) were installed in the prestressed, precast beam to continuously log the behaviour of the beam in response to concrete hydration, daily temperature variations and destressing. The measured temperatures and strains were then analysed to determine whether any significant temperature effects existed in the beam whilst still in the prestressing bed.

Three VWSGs and a total of 21 thermistors were installed. The VWSGs were installed in the top and bottom of the beam (as shown in Figure 3) to investigate whether different strains occurred due to the differing geometry, number of strands and possible temperature differences. The VWSGs contained their own temperature sensors allowing the recorded strains to be accurately temperature compensated. Fourteen thermistors were installed along the same cross-section as the VWSGs, 7 along the inner reinforcing and 7 along the outer reinforcing. Temperature profiles along the vertical height of the beam and temperature variations between the inner and outer concrete could therefore be analysed. The remaining seven thermistors were placed longitudinally along the bottom of the beam at two metre centres beginning at 2 metres from centre of the beam and ending 12 metres away from the middle to determine whether the cross-sectional temperatures were similar throughout the length of the beam. Recording started as the concrete was poured.

The FBGs were placed as close to the VWSGs as possible. The FBGs, were spaced at one metre intervals within the fibre optic cable. A fibre optic cable with 20 FBG sensors was used by splitting the cable into three separate cable arrays. Sixteen FBGs sensors were placed longitudinally along the bottom middle of the beam as indicated by the dashed line in Figure 3(c) beginning in the centre with the far end 16 metres from the middle of the beam. The remaining four FBGs were placed along the top prestressing strand, two on the Western side and two on the Eastern side. The positioning is indicated in Figure 3(a).

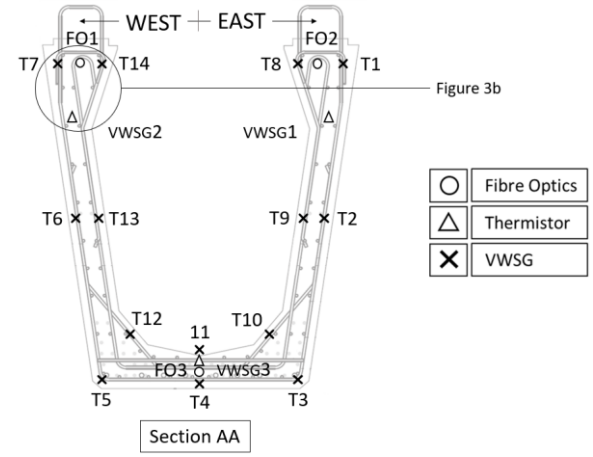

a) Beam cross-section (section AA)

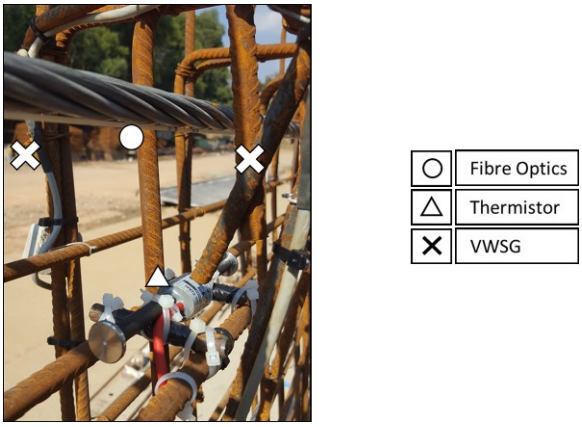

b) Example of instrument installation

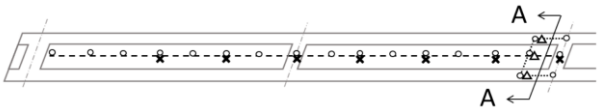

c) Plan on half of beam

Fig. 3. Instrumentation layout.

3 Results and Discussion

The thermistors and VWSG's were logged continuously for 9 days from the time the concrete was placed. This period included the de-stressing of the prestressed cables. The temperature and strain readings observed are discussed below.

3.1. Temperature Data

The temperatures recorded in four locations of the beam cross-section are shown in Figure 4. It can be noted that temperatures at the top of the beam (T7) show greater variation than temperatures at the bottom (T4). Thermistors T5 and T6 in the cross-section plot within the minimum and maximum temperature variations of T4 and T7. Temperatures for only four thermistors are shown as the rest show a similar trend. Instantaneous temperature differences of up to 10.5 °C between the top

and bottom sections were recorded. Temperature peaks occur at different times depending on the position in the beam, resulting in thermally induced strain gradients.

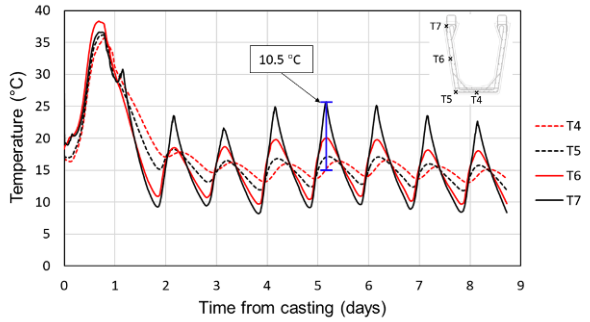

Fig. 4. Beam temperature on outer surface.

The temperature difference between the inner and outer thermistors is shown in Figure 5. Temperatures between the inner and outer thermistors are very similar except when the maximum temperatures are reached. A temperature difference of up to 3.5 °C existed between T7 and T14 (at the top of the beam) for the maximum temperature of the day. Thermistors T5 and T12 (at the bottom of the beam) were chosen to represent the minimum temperature variations as T12 exhibited a slightly different temperature plot to the rest. Although the maximum temperature differences between T5 and T12 is less than that for the thermistors at the top (1 °C vs 3.5 °C), the instantaneous difference is higher, at 3.6 °C. This is caused by the rapid increase in temperature at T12, whereas the temperature increase for T5 is more gradual. T12 was located on the bottom inner corner of the beam, and therefore showed a significant temperature increase as soon as the sun was high enough to shine directly onto the inside concrete face. The geometry and orientation of the beam is such that there is not a uniform exposure to environmental factors. This has a significant effect on the temperature distributions within the beam.

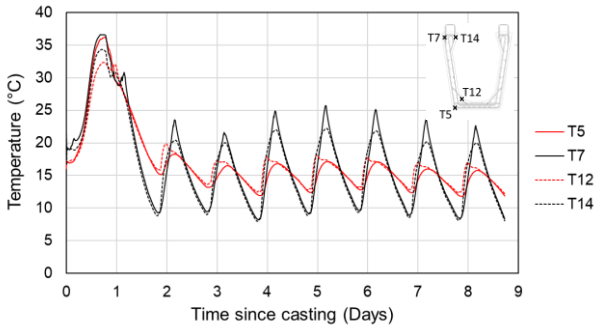

Fig. 5. Temperature differences between the inner and outer surface.

Vertical temperature profiles for the maximum and minimum temperatures are shown in Figure 6. Non-linear temperature profiles are displayed by the west outer and east inner side. This behaviour is a result of the North-South orientation of the beam. Therefore, the west outer and east inner side receive direct sunlight in the afternoon when the temperatures are at their highest. This resulted in the top thermistors recording the highest temperatures. The west inner and east outer side were completely in shade when the maximum temperature was reached resulting in a linear temperature profile. The greatest temperature difference between the top and bottom of the beam during the coldest temperatures was 4 °C (along the east outer side) and 8.5 °C (along the west outer side) during the hottest temperatures.

The behaviour for minimum temperatures is almost opposite to that of maximum temperatures in that the east outer side now shows the most non-linear temperature profile whereas the west outer side is now linear. The behaviour of these temperature profiles can be attributed to the protection against the colder night temperatures as well as the thickness of the concrete. Both inner sides show much warmer temperatures at the bottom, since the concrete is both thicker at the inner corners and is most protected against wind, resulting in less heat loss than the top inner concrete. In all cases, the bottom temperatures are higher than the top since the concrete is thicker at the corners and less exposed to wind than the top section.

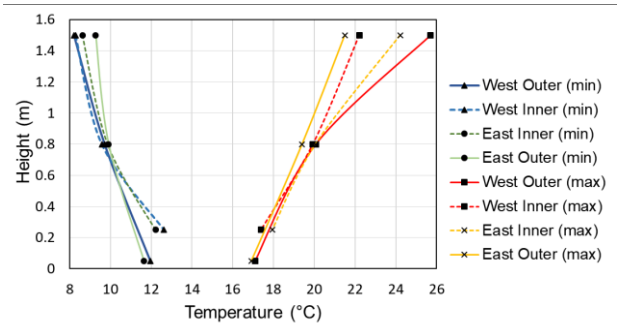

Fig. 6. Vertical temperature profiles.

3.2 Strain Data

Strains and temperatures were monitored continuously from the time of casting using VWSGs. The temperatures correlate to those measured using the thermistors, and could therefore be used to temperature compensate the strains, resulting in the actual concrete strain, which could then be further separated into mechanical strain.

The measured strains include the total concrete strain as well as thermal effects in the VWSG due to the steel vibrating wire in the gauge having a different coefficient of thermal expansion than concrete. The total strains in the concrete could therefore be calculated using equation 1 provided by the manufacturer of the VWSG:

$$\mu_{total} = (R_1 - R_0) + (T_1 - T_0)\,(C_1) \qquad (1)$$

Where R_0 = initial strain, R_1 = final strain, T_0 = initial temperature, T_1 = final temperature, C_1 = coefficient of thermal expansion of the VWSG. The total strains experienced by the beam are shown in Figure 7. Tensile (positive) strains occur during the exothermic reaction of concrete hydration followed by smaller strain variations

due to daily temperature changes. The average change in total strain for the beam cross-section, excluding the strains caused by concrete hydration, was approximately 65 με.

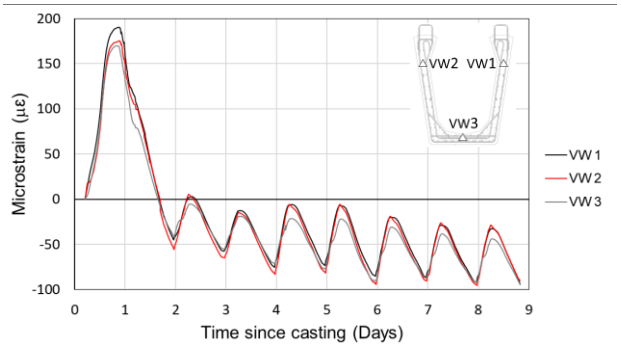

Fig. 7. Strain caused by temperature variation.

Although no external loads are applied to the beam, mechanical strains are present in the beam due to the geometry of the beam and the resulting difference in thermal strains between different sections. The resulting mechanical strains, based on the concrete coefficient of thermal expansion can be calculated using equation 2:

$$\mu_{\text{mechanical}} = (R_1 - R_0) + (T_1 - T_0)(C_1 - C_2) \qquad (2)$$

Where C_2 = coefficient of thermal expansion of the concrete. The mechanical strains are shown in Figure 8. Initial tensile strains are recorded during concrete hydration due to the exothermic reaction, after which the top and bottom sections show opposite behaviour once the concrete has set and begins to cool. The mechanical strains differ between the top (1 and 2) and the bottom (3) VWSGs. The opposing strains between the top and bottom of the beam cross-section occurs because of the different daily temperature variations. The top part of the beam is exposed to a greater temperature range than the bottom part. As a result, different thermal strains occur at the top and bottom. With a general temperature rise, the top of the beam will expand more than the bottom (which is exposed to a lower temperature range temperature). The top therefore goes into compression and the bottom into tension to reach a state of equilibrium between the two thermal strains. The reverse applies to an overall temperature decrease, with similar reasoning.

A closer look at the temperature variations along with the resulting mechanical strains can be seen Figure 9. The minimum temperatures at the top of the beam occurred at around 09:00, whereas the minimum temperatures in the bottom of the beam occurred at around 11:30. The maximum temperatures occurred at around 17:00 and 21:00 for the top of the beam and the bottom part of the beam respectively. The minimum and maximum temperatures occur later than expected as the ambient temperatures peaked at only roughly 16:00 with the coldest time being at around 08:00 due to the location of the precasting yard.

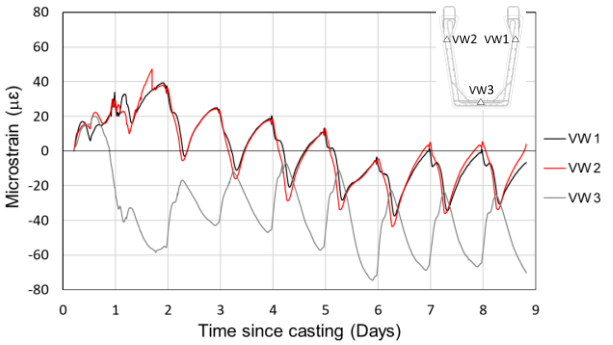

Fig. 8. Mechanical strain from VWSG.

The strains in the beam respond closely to the temperature variations in the top of the beam as those temperatures vary more than the temperatures in the bottom of the beam. It can be seen that a temperature increase in the top of the beam causes the top to go into compression and the bottom to go into tensions as discussed previously. The VWSG can therefore be used to continuously monitor the internal stresses caused within the beam due to daily vertical temperature gradients.

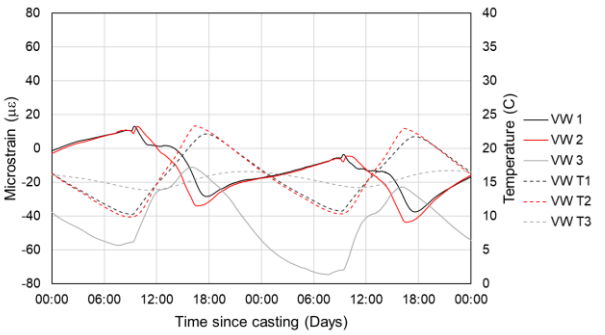

Fig. 9. Mechanical strains in the beam between day 4 and 6.

3.3 Strains after Destressing

The magnitudes of the strains before destressing can be compared to the strains caused when the prestressing strands are cut. Figure 10 from the VWSGs and Figure 11 from the fibre optics show the observed total strains during the process of destressing, 11 days and 18 hours after casting. Both sensors show the same trends. Due to a faulty power source the start of the destressing was not captured by the fibre optics. Therefore, the strains from the fibre optics were calibrated to be equal to the strains from the VWSG corresponding to the time at the fibre optic logger began to record.

Each small increase in compressive strain correlates to a strand being cut. The prestressing bed consisted of three prestressed beams all stressed by the same strands between two anchors. To keep the stresses evenly distributed, between one and four strands were cut at a time, starting from one end of the prestressing bed, followed by the strands between the first and second beam, then the strands between the second and third beam to end at the far end of the third beam. This pattern continued back and forth between the anchors until all

strands were cut. Therefore, smaller increases in compression correspond to strands being cut which were not adjacent the instrumented beam (the central beam).

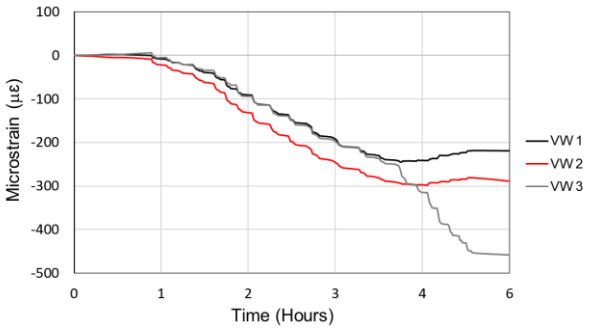

Fig. 10. VWSG strain during destressing.

The vertical temperature profiles caused by daily temperature variations induced mechanical strains of up to 62 με in the beam (Figure 8), which is 14% of the bottom compressive strains (VWSG 3) caused by destressing, and 28% of the final top compressive strains (VWSG 1) caused by destressing.

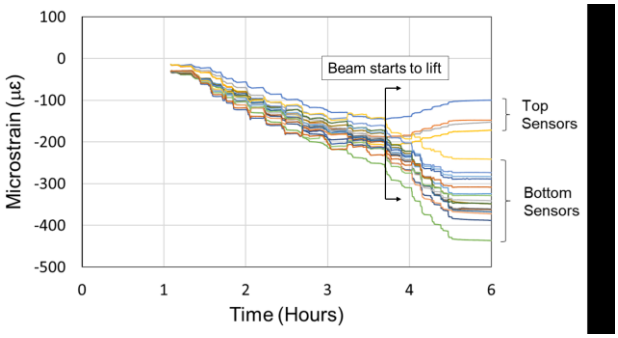

Fig. 11. Strain readings from FBG's during destressing.

There is a clear point shown by both graphs where the top sensors show a reduction in compressive strains. This behaviour occurs once enough strands have been cut to transfer sufficient compressive stress into the bottom of the beam to lift the beam up, i.e. to overcome the self-weight of the beam. Once the curvature is introduced, the compression in the top decreases, and the rate at which the bottom compresses increases after each successive strand is cut.

Figure 12 indicates the changes in strain along the length of the beam. The compressive force introduced into the beam after a strand is cut is not uniform throughout the length of the beam as some strands are debonded up to a certain distance from the edge of the beam. The prestressing force is therefore at its highest in the centre of the beam where all strands are bonded, and lowest at the end of the beam where 22 of the 54 strands are unbonded.

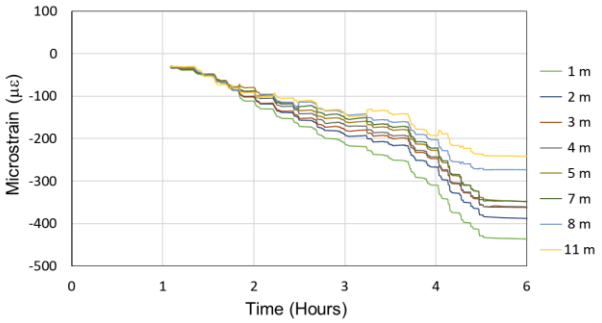

Fig. 12. Strains during destressing at different distances from the centre of the beam.

The difference in observed compressive strains along the length of the beam following destressing can be compared to theoretical calculations of the expected stresses after destressing. These compressive stresses are a combination of the overall compressive force from the prestressing strands, the moment created by the strands due to their eccentric location, and the self-weight of the beam. Furthermore, the combination of these three forces changes along the length of the beam as some prestressing strands are debonded certain lengths from the end of the beam and will therefore not transfer compressive forces along the entire length of the beam.

The theoretical force from the strands (consisting of the axial compression and moment caused by their eccentricity) were combined to calculate the theoretical stress as shown in Figure 13. The reduction in stress at each step correlate to an increased number of debonded strands towards the end of the beam.

The self-weight of the beam would result in tension at the bottom of the beam and therefore reduces the compressive stresses caused by prestressing. Combining the theoretical self-weight tensile stresses with the theoretical compressive prestress stresses result in the expected theoretical stresses after destressing as shown in Figure 13. There is a close correlation between the measured and theoretical stresses. Differences between the stresses are due to prestress losses caused by creep, shrinkage and strand relaxation as well as the quality of the bond between the fibre optic and the concrete.

However, the fact that the observed stresses plot closely to the theoretical stresses indicates that the fibre optics can successfully monitor the stresses during destressing and will therefore be useful in calculating the actual prestress losses which can then be compared to the expected design prestress losses.

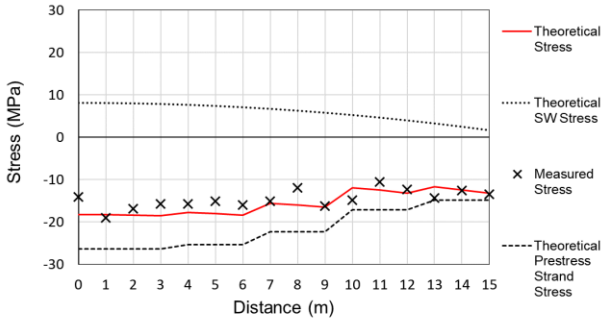

Fig. 13. Stresses after destressing at different distances from the centre of the beam.

4 Conclusions

A prestressed precast concrete beam was instrumented to investigate the effect of temperature variations on strain. Temperature variations existed along the vertical profile of the beam as well as through the thickness of the concrete section. Non-linear temperature variations were observed which can cause non-linear strains in precast beams which will differ depending on the geometry of the beam and the environmental conditions. The highest total strains before destressing were recorded during the higher temperatures of concrete hydration. However, the mechanical strains, which cause internal stresses, were most evident during daily temperature cycles when a temperature differences exists between the top and the bottom section of the beam.

Vertical temperature profiles induced mechanical strains of up 14% of the bottom compressive strains (VWSG 3) caused by destressing, and 28% of the final top compressive strains (VWSG 1 and 2) caused by destressing. Thermal effects before destressing should therefore be included in the design of prestress losses.

The internal stresses caused by daily temperature differentials in the beam and the time of destressing may affect the prestress losses and should therefore be investigated in future research.

The strains caused by destressing can be monitored using fibre optics which can be used to calculate prestress losses to compare the actual prestress losses with the prestress losses assumed for design purposes.

The monitoring techniques used here can track the performance of the structure and assist with informed decision making for its maintenance throughout the lifetime of the structure.

The following organizations are gratefully acknowledged for their assistance during the course of the study: Alborada Research Fund; The Concrete Institute; University of Pretoria; University of Cambridge; ARQ Consulting Engineers; Civilcon; Livierio Group.

References

1. P.J. Barr, J.F. Stanton, M.O. Eberhard, J. Bridge Eng. **10.2**, 186-194 (2005)
2. M. Emerson, TRRL Report LR 561, Berkshire, UK (1973)
3. J.H. Emanuel, J.L. Hulsey, J. Struct. Div. **104.1**, 65-78 (1978)
4. J.B. Kennedy, M.H. Soliman, J. Struct. Eng. ASCE **113.3**, 475–482 (1987)
5. C.W. Roeder, S. Moorty, J. of Struct. Eng. **118.4**, 1090-1105 (1992)
6. J.A. Gilland, W.H. Dilger, Can. J. Civil Eng. **24.6**, 941–950 (1997)
7. M.A. Pisani, Eng. Struct. **26.10** 1349–1363 (2004)
8. D. Li, M.A. Maes, W.H. Dilger, Can. J. Civil Eng. **31**, 813-825 (2004)
9. J. Lee, I. Kalkan, Adv. Struct. Eng. **15.3**, 447-459 (2012)
10. J. Lee, Eng. Struct. **42**, 1-8 (2012)
11. M. Emerson, TRRL Report LR 561, Berkshire, UK (1973)
12. H.M. Dwairi, M.C. Wagner, M.J. Kowalsky, P. Zia, Constr. Build. Mat. **24.11**, 2294-2311 (2010)
13. R.A. Imbsen, D.E. Vandershaf, R.A. Schamber, R.V. Nutt, NCHRP Report 276 (1985)
14. M. Emerson, TRRL Report LR 765, Berkshire, UK (1977)
15. L.J. Butler, N. Gibbons, P. He, C. Middleton, M.Z.E.B. Elshafie, Constr. Build. Mat. **126** 894-912 (2016)
16. P.J. Barr, F. Angomas, J. Perf. Constr. Fac. **24.6**, 603-609 (2010)
17. K.A. Riding, J.L. Poole, K.J. Folliard, M.C.G. Juenger, A.K. Schindler, ACI Mat. J. **106.5**, 448-454 (2009)
18. Z. Chen, Z. Liu, G. Sun, J. Mat. Civil Eng. **23.9**, 1265-1271 (2011)
19. M.K. Tadros, N. Omaishi, S.J. Seguirant, J.G. Gallt, NCHRP Report 496 (2003)
20. Y. Liu, W. Zuk, PCI J. 1-85 (1963)